Steroids 76 (2011) 1389–1396

Contents lists available at ScienceDirect

Steroids

journal homepage: www.elsevier.com/locate/steroids

Cytotoxic and haemolytic steroidal glycosides from the Caribbean sponge *Pandaros acanthifolium*

Erik L. Regalado [a,*], Tom Turk [b,*], Deniz Tasdemir [c], Manca Gorjanc [b], Marcel Kaiser [d,e], Olivier P. Thomas [a], Rogelio Fernández [f], Philippe Amade [a]

[a] Laboratoire de Chimie des Molécules Bioactives et Arômes, UMR 6001 CNRS, University of Nice-Sophia Antipolis, Faculté des Sciences Parc Valrose, 06108 Nice Cedex 2, France
[b] Department of Biology, Biotechnical Faculty, University of Ljubljana, Večna Pot 111, 1000 Ljubljana, Slovenia
[c] Department of Pharmaceutical and Biological Chemistry, School of Pharmacy, University of London, 29-39 Brunswick Square, London WC1N 1AX, United Kingdom
[d] Swiss Tropical and Public Health Institute, Socinstrasse 57, P.O. Box, 4002 Basel, Switzerland
[e] University of Basel, Petersplatz 1, 4051 Basel, Switzerland
[f] Pharmamar, Poligono Industrial La Mina Norte, Avenida de los Reyes, 1, 28770 Colmenar Viejo, Spain

ARTICLE INFO

Article history:
Received 16 June 2011
Received in revised form 17 July 2011
Accepted 19 July 2011
Available online 26 July 2011

Keywords:
Marine sponge
Pandaros
Steroidal glycosides
Cytotoxic
Antiprotozoal
Haemolytic

ABSTRACT

Six new steroidal saponins, pandarosides K–M (**1**–**3**) and their methyl esters (**4**–**6**), were isolated as minor components, after a careful chemical reinvestigation of the Caribbean sponge *Pandaros acanthifolium*. Their structures were established on the basis of spectroscopic analyses and comparison with the data obtained from previous metabolites of this family. All new compounds showed moderate to weak activity against four parasitic protozoa. Additionally, these compounds and previously reported pandarosides and acanthifoliosides were tested on three human tumour cell lines, and their haemolytic and liposome permeabilizing activity were assessed. Two pandarosides exhibited moderate to strong cytotoxic effect, while three acanthifoliosides showed strong haemolytic activity.

1. Introduction

Even if marine sponges of the order Poecilosclerida have been widely investigated, they still represent a rich source of new secondary metabolites [1]. This order is well known to produce a large diversity of complex guanidine alkaloids [2]. However, only acanthifolicin, an episulfide-containing polyether carboxylic acid, had been isolated from species of the genus *Pandaros* [3]. Recently, we reported the presence of novel steroidal saponins, namely pandarosides and acanthifoliosides, from a specimen of *Pandaros acanthifolium* collected in the Caribbean sea [4–6]. Pandarosides are characterized by the occurrence of a rare 2-hydroxycyclopent-2-enone D ring with a *cis* C/D ring junction and a C-23 ketone, while acanthifoliosides contain a less oxidized D ring bearing additional sugar residues at C-15 or C-16. Some of these saponins, such as pandaroside G (**7**) and its methyl ester (**8**), were found to exhibit high antiprotozoal bioactivities [5]. Additionally, the strongest haemolytic activity was observed in aqueous extracts from *P. acanthifolium* out of 66 extracts of Caribbean marine sponges [7].

An antitumour screening study also showed that the crude extract of *P. acanthifolium* had significant activity. This prompted us to reinvestigate the bioactive saponin-rich subfraction, which led to the isolation of six new minor steroidal glycosides (**1**–**6**) containing the rare oxidized D-ring characteristic of pandarosides. Their structures were elucidated by spectroscopic studies including 1D- and 2D-NMR experiments (COSY, HSQC, HMBC, NOESY), HRESI-MS analyses and the comparison of their spectral data with those of known analogues. Together with previously known pandarosides and acanthifoliosides, their *in vitro* antitumour activity (against lung, colon and breast cancer cell lines) as well as haemolytic and membrane-permeabilizing activities were assessed. The *in vitro* inhibitory activity of the new metabolites against a small panel of parasitic protozoa, i.e. *Trypanosoma brucei rhodesiense*, *Trypanosoma cruzi*, *Leishmania donovani*, and *Plasmodium falciparum*, was also evaluated.

2. Experimental

2.1. General

Optical rotations were measured on Perkin–Elmer 343 polarimeter equipped with a 10-cm microcell. UV/CD spectra were

* Corresponding authors. Tel.: +33 492076134; fax: +33 492076599.
E-mail address: erikluis18@gmail.com (E.L. Regalado).

0039-128X/$ - see front matter © 2011 Elsevier Inc. All rights reserved.
doi:10.1016/j.steroids.2011.07.010

performed using a JASCO J-810 spectropolarimeter. IR spectra were obtained with a Perkin–Elmer Paragon 1000 FT-IR spectrometer. UV measurements were performed on a Varian Cary 300 Scan UV–visible spectrometer. Electrospray ionization (ESI) mass spectra were obtained with a Bruker Esquire 3000 Plus spectrometer in the positive or negative mode. High resolution mass spectra (HRESIMS) were obtained from a LTQ Orbitrap mass spectrometer (Thermo Finnigan). NMR experiments were performed on a Bruker Avance 500 MHz spectrometer. Chemical shifts (δ in ppm) are referenced to the carbon (δ_C 49.0) and residual proton (δ_H 3.31) signals of CD_3OD, the solvent with multiplicity (s singlet, d doublet, t triplet, m multiplet). HPLC separation and purification were carried out on a Waters 600 system equipped with a Waters 996 Photodiode Array detector coupled with a Sedex 55 ELSD (SEDERE, France), and a Waters 717 plus Autosampler. TLC was performed with Kieselgel 60 F_{254} (Merck glass support plates) and spots were detected after spraying with 10% H_2SO_4 in EtOH reagent and heating.

2.2. Biological material

The marine sponge was collected off Martinique Island in summer 2003 by SCUBA diving (Canyons de Babodie 14°45,982 N, 61°11,902 W). A voucher specimen (ORMA8362) identified by Dr. Jean Vacelet, has been deposited in the Centre d'Océanologie de Marseille (Endoume, France). The sponge was kept frozen from collection until the extraction process.

2.3. Extraction and isolation

The frozen sponge (536 g) was cut into pieces of about 1 cm^3 and extracted with MeOH/CH_2Cl_2 1:1 at room temperature yielding 20 g of crude extract after solvent evaporation. The crude extract was fractionated by RP-C_{18} flash chromatography (elution with a decreasing polarity gradient of H_2O/MeOH from 1:0 to 0:1, then MeOH/CH_2Cl_2 from 1:0 to 0:1). The H_2O/MeOH 1:3 (220 mg) fraction was then subjected to RP-C_{18} semi-preparative HPLC (Phenomenex, Luna C_{18}, 250 × 10 mm, 5 μm) with a gradient of H_2O/MeOH/TFA (flow 3.0 mL min^{-1} from 28:72:0.1 to 20:80:0.1) and the subsequent mixtures were finally purified by analytical HPLC (Phenomenex, Gemini C_6-phenyl, 250 × 3 mm, 5 μm) with isocratic mobile phases (H_2O/CH_3CN/formic acid, 63:37:0.1 and 50:50:0.1, flow 0.5 mL min^{-1}) to afford pure compounds **1** (1.5 mg, 0.3 × 10^{-3}% w/w), **2** (1.4 mg, 0.3 × 10^{-3}% w/w), **3** (1.6 mg, 0.3 × 10^{-3}% w/w), **4** (1.4 mg, 0.3 × 10^{-3}% w/w) **5** (1.3 mg, 0.3 × 10^{-3}% w/w) and **6** (1.4 mg, 0.3 × 10^{-3}% w/w).

2.3.1. Pandaroside K (1): 3β-O-[β-glucopyranosyl-(1 → 2)-β-glucopyranosyloxyuronic acid]-16-hydroxy-5α,14β-ergost-16-ene-15,23-dione

White amorphous solid; $[\alpha]_D^{24}$ +28.7 (*c* 0.05, MeOH); UV (MeOH): λ_{max} (log ε) 264 (4.27) nm; CD (MeOH, *c* 3.8 × 10^{-4} M) θ (λ_{max} nm) −5 (220), +13 (262), −4 (289), +4 (327) mdeg; IR (thin film): ν_{max} 3490, 1695, 1639, 1196 cm^{-1}; ^1H and ^{13}C NMR data (see Table 1); HRESIMS (+): *m/z* 805.42084 $[M+Na]^+$ (calcd for $C_{40}H_{62}NaO_{15}$, 805.42117, Δ −0.41664 ppm).

2.3.2. Pandaroside L (2): 3β-O-[β-glucopyranosyloxyuronic acid]-16-hydroxy-5α,14β-poriferasta-7,16-diene-15,23-dione

White amorphous solid; $[\alpha]_D^{20}$ +6.6 (*c* 0.05, MeOH); UV (MeOH): λ_{max} (log ε) 264 (3.83) nm; CD (MeOH, *c* 5.0 × 10^{-4} M) θ (λ_{max} nm) −3 (220), +10 (262), −4 (285), +4 (327); IR (thin film): ν_{max} 3410, 1695, 1679, 1195 cm^{-1}; ^1H and ^{13}C NMR data (see Table 1); HRESIMS (+): *m/z* 655.35864 $[M+Na]^+$ (calcd for $C_{35}H_{52}NaO_{10}$, 655.36053, Δ −2.87245 ppm).

2.3.3. Pandaroside M (3): 3β-O-[α-L-rhamnopyranosyl-(1 → 4)-β-glucopyranosyloxyuronic acid]-16-hydroxy-5α,14β-cholest-16-ene-15,23-dione

White amorphous solid; $[\alpha]_D^{20}$ −22.1 (*c* 0.14, MeOH); UV (MeOH): λ_{max} (log ε) 264 (3.92) nm; CD (MeOH, *c* 3.9 × 10^{-4} M) θ (λ_{max} nm) −8 (220), +7 (262), −3 (289), +4 (327) mdeg; IR (thin film): ν_{max} 3340, 1725, 1664, 1199, 1132 cm^{-1}; ^1H and ^{13}C NMR data (see Table 1); HRESIMS (+): *m/z* 775.40093 $[M+Na]^+$ (calcd for $C_{39}H_{60}NaO_{14}$, 775.40113, Δ 0.65753 ppm).

2.3.4. Methyl ester of pandaroside K (4)

White amorphous solid; $[\alpha]_D^{20}$ +18.8 (*c* 0.11, MeOH); ^1H NMR (500 MHz, CD_3OD) for the uronic residue: δ 4.60 (d, *J* = 7.4 Hz, H-1′), 3.44 (t, *J* = 7.5 Hz, H-2′), 3.57 (m, H-3′ and H-4′), 3.85 (d, *J* = 9.0 Hz, H-5′), 3.76 (s, CH_3O–); ^{13}C NMR (125 MHz, CD_3OD) for the uronic residue: 102.1 (C-1′), 82.9 (C-2′), 73.0 (C-3′), 77.3 (C-4′), 76.5 (C-5′), 171.4 (C-6′), 53.0 (CH_3O–); HRESIMS (+): *m/z* 819.42085 $[M+Na]^+$ (calcd for $C_{41}H_{64}NaO_{15}$, 819.42052, Δ −1.18400 ppm).

2.3.5. Methyl ester of pandaroside L (5)

White amorphous solid; $[\alpha]_D^{20}$ +12.4 (*c* 0.05, MeOH); ^1H NMR (500 MHz, CD_3OD) for the uronic residue: δ 4.44 (d, *J* = 7.8 Hz, H-1′), 3.17 (dd, *J* = 9.0 and 8.0 Hz, H-2′), 3.37 (t, *J* = 9.0 Hz, H-3′), 3.51 (t, *J* = 9.0 Hz, H-4′), 3.84 (d, *J* = 9.0 Hz, H-5′), 3.77 (s, CH_3O–); ^{13}C NMR (125 MHz, CD_3OD) for the uronic residue: 102.8 (C-1′), 75.0 (C-2′), 77.5 (C-3′), 73.2 (C-4′), 76.7 (C-5′), 171.6 (C-6′), 52.9 (CH_3O–); HRESIMS (+): *m/z* 669.37041 $[M+Na]^+$ (calcd for $C_{36}H_{54}NaO_{10}$, 669.37050, Δ −0.60880 ppm).

2.3.6. Methyl ester of pandaroside M (6)

White amorphous solid; $[\alpha]_D^{20}$ −20.8 (*c* 0.14, MeOH); ^1H NMR (500 MHz, CD_3OD) for the uronic residue: δ 4.55 (d, *J* = 7.5 Hz, H-1′), 3.37 (t, *J* = 7.8 Hz, H-2′), 3.50 (dd, *J* = 9.1 and 8.5 Hz, H-3′), 3.49 (t, *J* = 9.0 Hz, H-4′), 3.84 (d, *J* = 9.2 Hz, H-5′), 3.77 (s, CH_3O–); ^{13}C NMR (125 MHz, CD_3OD) for the uronic acid residue: 100.7 (C-1′), 78.9 (C-2′), 73.1 (C-3′), 78.7 (C-4′), 76.6 (C-5′), 171.3 (C-6′), 52.9 (CH_3O–); ESIMS (+): *m/z* 789.4 $[M+Na]^+$.

2.4. Protocol for the determination of absolute configuration of sugar units

2.4.1. Methanolysis of pandarosides

Compounds **1**, **3**, and **5** (0.30 mg) were dissolved in a HCl (7 N, 1.0 ml)–MeOH solution (Supelco, USA) and heated at 75 °C for 4 h. The reaction mixture was neutralized with $NaHCO_3$, evaporated to dryness, and then partitioned between $CHCl_3$ and H_2O. The H_2O layer was dried under reduced pressure to afford a mixture of methyl glycosides.

2.4.2. Derivatization of the hydrolyzate for GC analysis

The methanolysis products were dissolved in a mixture of dry CH_2Cl_2/pyridine (1:1) and an excess of acetic anhydride was added. The reaction was stirred at 25 °C for 8 h. Then, the mixture was directly dried and dissolved in AcOEt for GC analysis.

2.4.3. Chiral GC analysis

GC analysis was carried out on a Chirasil-L-Val Alltech capillary column (25 m × 0.25 mm, i.d.), using a Hewlett Packard Mass Selective Detector 5972 series. A temperature gradient system was used for the oven, starting at 100 °C for 3 min and increasing up to 200 °C at a rate of 10 °C/min. Peaks of the hydrolyzate of pandarosides and sugar standards were detected at 15.3 min (D-glucose, Glc), 12.1 min (D-glucuronic acid, GlcUA), and 11.5 min (L-rhamnose, Rha). Because some retention times fluctuated, the identity of the enantiomers was confirmed by injection

Table 1
^{1}H (500 MHz) and ^{13}C (125 MHz) NMR data (CD_3OD) for compounds **1**–**3**: δ in ppm, multiplicity (J in Hz).

C	**1**		**2**		**3**	
	δ ^{1}H	δ ^{13}C	δ ^{1}H	δ ^{13}C	δ ^{1}H	δ ^{13}C
1β	1.68, m	37.4	1.79, m	37.7	1.65, m	37.4
1α	0.86, m		0.96, m		0.86, m	
2α	1.83, m	30.0	1.85, m	30.1	1.86, m	30.0
2β	1.49, m		1.61, m		1.50, m	
3	3.64, m	80.8	3.49, m	79.8	3.64, m	78.9
4α	1.73, m	35.5	2.42, m	39.2	1.72, m	35.3
4β	1.27, m		2.21, m		1.28, m	
5	1.04, m	45.6	1.23, m	43.6	1.03, m	45.6
6α	1.34, m	30.2	2.99, m	30.3	1.35, m	30.3
6β	1.29, m		1.95, m		1.30, m	
7α	2.17, m	31.2	5.42, dd (5.0, 2.0)	123.4	2.17, m	31.4
7β	1.65, m				1.66, m	
8	1.93, m	35.0		141.5	1.93, m	35.2
9	0.88, m	45.8	2.01, m	31.2	0.87, m	45.9
10		38.2		40.1		38.3
11β	1.37, m	19.9	1.43, m	19.2	1.38, m	19.9
11α	1.18, m		1.14, m		1.16, m	
12β	1.55, m	32.6	1.59, m	31.8	1.55, m	32.6
12α	1.47, m		1.41, m		1.46, m	
13		43.8		43.9		43.6
14	1.83, d (4.5)	56.1	1.89, brs	54.3	1.83, d (4.5)	56.2
15		206.0		205.8		206.0
16		151.4		151.5		151.4
17		154.9		153.4		154.7
18	1.15, s	25.8	1.21, s	25.7	1.16, s	25.9
19	0.81, s	11.1	1.04, s	18.0	0.80, s	11.1
20	2.90, m	27.4	2.91, m	27.4	2.83, m	28.1
21	1.16, d (7.0)	18.0	1.17, d (6.6)	17.9	1.15, d (4.5)	18.0
22a	3.05, dd (18.0, 8.9)	47.3	2.97, m	49.0	2.85, m	48.1
22b	2.79, dd (17.8, 4.5)		2.82, m			
23		215.8		215.7		212.3
24	2.34, m	54.3	2.23, ddd (10.4, 7.4, 3.8)	61.8	2.31, d (6.9)	53.3
24^{1}a	1.01, d (7.1)	12.9	1.57, m	22.4		
24^{1}b			1.53, m			
24^{2}			0.77, t (7.4)	12.3		
25	1.90, m	31.2	1.88, m	30.9	2.09, m	25.7
26/27	0.86, d (6.8)	19.2	0.89, d (6.6)	20.1	0.89, d (6.5)	22.9
	0.91, d (6.8)	21.6	0.90, d (6.6)	21.6	0.90, d (6.5)	22.9
1′	4.57, d (7.8)	101.8	4.44, d (7.8)	102.8	4.54, d (7.8)	100.5
2′	3.45, m	82.6	3.18, dd (9.2, 7.8)	75.0	3.37, t (9.4)	79.0
3′	3.58, t (9.7)	72.7	3.36, t (8.8)	77.4	3.51, m	73.2
4′	3.56, t (9.6)	77.3	3.51, t (9.2)	73.4	3.49, m	78.5
5′	3.77, m	76.4	3.77, d (9.5)	76.6	3.77, d (8.3)	76.8
6′		172.3		172.0		172.1
1″	4.53, d (7.8)	105.3			5.18, d (1.4)	102.1
2″	3.25, t (8.2)	76.2			3.91, dd (3.2, 1.4)	72.2
3″	3.38, t (8.7)	77.5			3.64, m	72.4
4″	3.33, m	71.4			3.38, t (9.4)	73.9
5″a	3.27, m	78.2			4.10, dq (9.4, 6.2)	69.8
5″b						
6″a	3.84, dd (11.8, 2.5)	62.7			1.22, d (6.4)	18.0
6″b	3.70, dd (11.8, 5.0)					

of a mixture of the sample and standards acetylated using the same protocol.

2.5. Antiprotozoal assays

In vitro antimalarial activity against erythrocytic stages of *P. falciparum*, trypanocidal activity against *T. b. rhodesiense* and *T. cruzi*, leishmanicidal activity against *L. donovani* and cytotoxicity assessments towards L6 cells (a primary cell line derived from mammalian (rat) skeletal myoblasts) were performed following the same protocol used in our previous paper [5].

2.6. Antitumour assays

A colorimetric assay using sulforhodamine B has been adapted for a quantitative measurement of cell growth and viability following the technique described in the literature [8]. The *in vitro* activity of the compounds was evaluated against three tumour cell lines, including lung carcinoma NSCLC A549, colon carcinoma HT29, and breast MDA-MB-231.

2.7. Haemolytic activity assay

Haemolytic activity of pandarosides and acanthifolioside families was tested on freshly prepared bovine erythrocytes by means of turbidimetric method as previously described by Macek and Lebez [9]. Briefly, citrated red blood cells were washed twice with 0.9% NaCl and centrifuged at 2500 rpm, and finally the procedure was repeated using the erythrocyte buffer (130 mM NaCl, 20 mM Tris–HCl, pH 7.4). Washed erythrocytes were suspended in the erythrocyte buffer to give an apparent absorption of 0.5 units at 700 nm. One mL of erythrocyte suspension was pipeted into

cuvette, different amounts of each tested compound in methanol were added and time course of haemolysis was monitored for 5 min at a constant temperature of 25 °C The rate of haemolysis was evaluated as $1/t_{50}$, the reciprocal value of time needed for a drop of apparent absorption from 0.5 to 0.25. HC_{50} was defined as the amount of each compound (μM) needed for 50% apparent absorption decrease of erythrocyte suspension in 60 s. All recordings were done in triplicates using Shimatzu double bean UV–visible spectrophotometer (Shimatzu, Japan).

2.7.1. Inhibition of haemolysis by osmoprotection

In order to get further insight to the mechanism of lysis a series of osmoprotectant compounds with increasing molecular weight were used (PEG 300, 600, 1450, 3350, 4000 and 8000). Osmoprotectants were added into erythrocyte suspensions and the time courses of haemolysis were monitored as described previously, but prolonged up to 10 min. The final concentration of osmoprotectants was 1 mM. All measurements were done in triplicate.

2.7.2. Preparation of small unilamellar vesicles (SUV)

SUV were prepared either with single lipid (sphyngomielin, SM) or palmitoyl oleoyl phosphatidylcholine (POPC) either with a mixture of the two lipids in 1:1 M ratio (POPC:SM). Lipids were dissolved in chloropharm and dried for 3 h under reduced pressure (Rotavapor, Büchi, Switzerland) until the lipid film was formed on the inner surface of rounded flask. Then, 1 mL of vesicle buffer (20 mM Tris–HCl, 140 mM NaCl, 1 mM EDTA, pH 8.0) and 15–20 glass beads were added into flask and shaked vigorously for 1–2 min using vortex apparatus. Obtained multilamellar vesicles were sonicated for 30 min by 10 s pulse intervals. Obtained SUV were incubated 45 min at 40 °C followed by centrifugation at 6000 rpm for 5 min. Prepared SUV were stored at 4 °C in a stock concentration of 10 mg/mL until further use.

2.7.3. Inhibition of haemolysis by small unilamellar vesicles (SUV)

Compounds **9**, **10** and **12** that proved to be haemolytic were further tested using different preparation of SUV. For each measurement 5 μL of SUV were added into 1 mL of erythrocyte suspension, immediately followed by compounds that have shown haemolytic activity in previous experiments. The time course of haemolysis was monitored for 10 min as described in Section 2.7. All experiments were done in triplicate.

2.7.4. Preparation of calcein loaded SUV

The preparation of SUV loaded with calcein was essentially carried out as described in Section 2.7.2, except that 80 mM calcein was included into SUV buffer. Untrapped calcein was separated from calcein loaded SUV by means of size exclusion chromatography using small column (10 mL total volume) loaded with Sephadex G-50 (General Electrics, Sweden).

2.7.5. Calcein release assay

Calcein release from calcein loaded SUV was monitored using Jasco FP-750 spectrofluorimeter (Jasco, Japan). If vesicles are permeabilized by a tested compound calcein is released and due to dilution and attenuated quenching effect the fluorescence increases. Samples in 1 mL cuvette were excitated at 485 nm and emission was monitored at 520 nm. Kinetics of calcein release was monitored for 10 min followed by addition of Triton X100 which caused a 100% calcein release. Amount of released calcein was calculated according to the following equation:

$$\%\ \text{of calcein released} = (F_{measured} = F_{min})/(F_{max} - F_{min}) \times 100$$

where $F_{measured}$ is maximal fluorescence after 10 min from the addition of each tested compound. F_{max} is the highest measured fluorescence after addition of Triton X100. F_{min} is initial fluorescence of intact calcein loaded SUV.

3. Results and discussion

3.1. Structural elucidation

The CH_2Cl_2/MeOH (1:1) extract of the Caribbean marine sponge *P. acanthifolium* was fractionated by RP-C_{18} flash chromatography and one fraction was further subjected to RP-C_{18} column chromatography and purified by RP-C_{18} semi-preparative HPLC and C_6-phenyl analytical HPLC to yield six new compounds **1**–**6** (Fig. 1), all of which were isolated as white amorphous solids. Their NMR

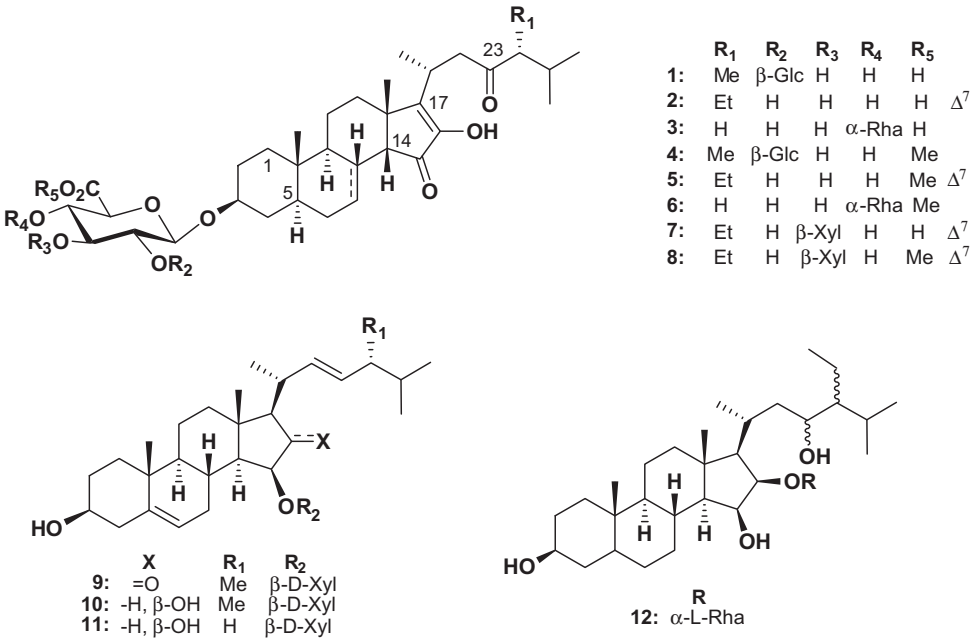

Fig. 1. Structure of pandarosides K–M (**1**–**3**) and G (**7**) with their methyl esters (**4**–**6** and **8**, respectively) and acanthifoliosides A–D (**9**–**12**).

spectroscopic features (Table 1) were similar and suggested one or two sugar residues linked to a steroidal moiety, closely related to previous pandarosides [4,5].

3.1.1. Pandaroside K (**1**)

The molecular formula of compound **1** was established as $C_{40}H_{62}O_{15}$ by the HRESIMS spectrum (*m/z* 805.42084 $[M+Na]^+$, Δ −0.41664 ppm). IR spectra showed the presence of hydroxyl and carbonyl groups in **1** (ν_{max} 3490, 1695 and 1639 cm^{-1}). The ^{13}C NMR and HSQC spectra of **1** confirmed the presence of 40 carbons, 28 corresponding to the aglycone part and 12 to the diosidic unit. The characteristic steroidal methyl signals at δ_H 1.15 (s)/δ_C 25.8 (H_3C-18), 0.81 (s)/11.1 (H_3C-19), 1.16 (d, 7.0 Hz)/18.0 (H_3C-21), 1.01 (d, 7.1 Hz)/12.9 (H_3C-24^1), 0.86 and 0.91 (d, 6.8 Hz)/19.2 and 21.6 (H_3C-26/H_3C-27) (Table 1), were consistent with an ergostane skeleton. The ^{13}C NMR signals at δ_C 56.1 (C-14), 206.0 (C-15), 151.4 (C-16), and 154.9 (C-17) confirmed the presence of the rare 2-hydroxycyclopent-2-enone D-ring, previously described for pandarosides [4,5] and two stemmosides [10]. The presence of the ketone (215.8 ppm) at C-23 of the side chain, was confirmed by the key H-20, H-22, H-24 and H-24^1/C-23 HMBC correlations (Fig. 2). The NMR data for the side chain was almost identical to the one of pandaroside F and its methyl ester, unique examples of 23-oxo ergostanes [5].

The sugar part of **1** was found to include two sugar units with the characteristic signals of anomeric protons at δ_H 4.57 and 4.53 (1H, d, *J* = 7.8 Hz, H-1′ and H-1″, respectively), one belonging to a glucuronic acid (GlcUA) with a characteristic signal at δ_C 172.3 ppm (C-6′), and the second sugar being a glucose (Glc) by comparison with literature values. The position of the GlcUA was deduced to be at C-3 position of the aglycone due to the HMBC correlation between H-1′ and C-3. The terminal Glc was linked to the GlcUA at C-2′ because of the H-1″/C-2′ HMBC correlation. The large *J* values of the signals H-1′ and H-1″ (d, 7.8 Hz) indicated their *O*-β-glycosidic linkages.

The relative stereochemistry of the aglycone part was found to be the same as for pandarosides A–J due to similar NOE correlations and ^1H–^1H coupling constants. At the same time, the CD spectrum of **1** showed two positive Cotton effects at 262 and 327 nm, which were assigned to the $\pi \rightarrow \pi^*$ and $n \rightarrow \pi^*$ transitions of the cyclopentenone D ring, respectively; as well as a negative Cotton effect at 289 nm, assigned to the $n \rightarrow \pi^*$ transition of the side-chain ketone. These signals were similar to those of previously reported pandarosides, suggesting the same absolute configurations for the aglycone and the side chain at C-24, these conclusions being obtained by comparison between experimental and TDDFT-calculated CD spectra of pandaroside A [4]. The absolute configurations of D-GlcUA and D-Glc were obtained by chiral GC analysis following acid methanolysis and acetylation of the sugar residues [11], and all NMR data of this diglycoside were similar to those of pandaroside A, B and J, exhibiting the same glycosidic sequence [4,5]. Thus, **1** was identified as 3β-*O*-[β-glucopyranosyl-(1 → 2)-β-glucopyranosyloxyuronic acid]-16-hydroxy-5α,14β-ergost-16-ene-15,23-dione.

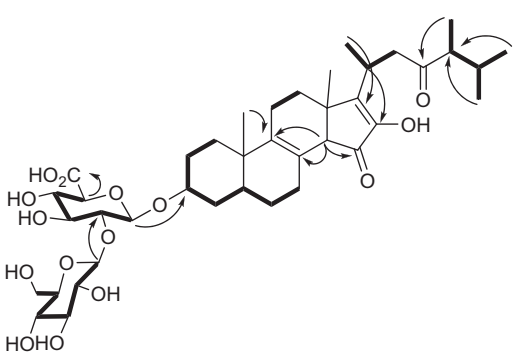

Fig. 2. Key HMBC (H → C) and H–H COSY (–) correlations for **1**.

3.1.2. Pandaroside L (**2**)

Compound **2** had a molecular formula of $C_{35}H_{52}O_{10}$, which was deduced from the HRESIMS spectrum (*m/z* 655.35864 $[M+Na]^+$, Δ −2.87245 ppm). A detailed comparison of NMR data of compound **2** with those of compound **1** revealed some differences in their aglycone part and the presence of only one anomeric proton/carbon signal at δ_H 4.44 (d, *J* = 7.8 Hz, H-1′)/δ_C 102.8 ppm. This indicated that only the GlcUA residue was present and connected at C-3, as previously described for pandarosides B and D [4]. Additionally, the methyl signals of **1** at δ_H 1.01 (d, *J* = 7.1 Hz, $\underline{H}_3$C-24^1)/δ_C 12.9 were replaced by the signals of an ethyl group at δ_H 1.57 and 1.53 (m, $\underline{H}_2$C-24^1)/22.4 ($H_2\underline{C}$-24^1) and 0.77 (t, *J* = 7.4 Hz, $\underline{H}_3$C-24^2)/12.3 ($H_3\underline{C}$-24^2) in **2**, which were consistent with a poriferastane/stigmastane skeleton. Besides, the occurrence of a trisubstituted double bond in **2** was deduced from the deshielded signals at δ_C 141.5 (C-8) and 123.4 (C-7)/δ_H 5.42 (dd, *J* = 5.0, 2.0 Hz, H-7). This unsaturation was placed at the C-7/C-8 position due to the H_2-6/H-7 COSY correlation, as previously described for pandaroside G [5]. In consequence, the structure of **2** was deduced to be 3β-*O*-[β-glucopyranosyloxyuronic acid]-16-hydroxy-5α,14β-poriferasta-7,16-diene-15,23-dione.

3.1.3. Pandaroside M (**3**)

The molecular formula of compound **3** ($C_{39}H_{60}O_{14}$) was established from the HRESIMS spectrum (*m/z* 775.40093 $[M+Na]^+$, Δ 0.65753 ppm). The ^1H and ^{13}C NMR data were also quite similar to those of pandaroside K (**1**) for the steroidal part. The differences were located on the side chain where the lack of the characteristic signal at δ_H 1.01 (d, *J* = 7.1, $\underline{H}_3$C-24^1) suggested that the methyl was absent from C-24. The AB signals at δ_H 3.05 (dd, *J* = 18.0, 8.9 Hz, H-22a) and 2.79 (dd, *J* = 17.8, 4.5 Hz, H-22b)/43.7 ($H_2\underline{C}$-22) were also replaced by a new signal at δ_H 2.85 (m, H-22a and b)/48.1 ($H_2\underline{C}$-22), which was consistent with a cholestane skeleton. Other changes were observed in the NMR spectra of one sugar residue. The GlcUA moiety was still present at C-3, but the second sugar residue was linked at C-4′ based on a H-1″/C-4′ HMBC correlation. The appearance of a new methyl signal at δ_H 1.22 (d, *J* = 6.4 Hz, $\underline{H}_3$C-6″) as well as the chemical shift and coupling constant of H-1″ anomeric proton at δ 5.18 (d, *J* = 1.4 Hz) suggested an α-rhamnose (Rha) as the terminal sugar [12]. The chiral GC analysis allowed us to propose the usual L absolute configuration for this sugar. All ^1H and ^{13}C NMR signals for this diglycoside were similar to those of pandaroside I [5]. On this basis, the structure of compound **3** was established as 3β-*O*-[α-L-rhamnopyranosyl-(1 → 4)-β-glucopyranosyloxyuronic acid]-16-hydroxy-5α,14β-cholest-16-ene-15,23-dione.

The molecular ion at *m/z* 819.42085 $[M+Na]^+$ in the HRESIMS established the molecular formula of compound **4** as $C_{41}H_{64}O_{15}$, which indicated the presence of an additional methylene unit in comparison with **1**. The ^1H and ^{13}C NMR data were very similar to those of **1** except for the new signals at δ_H 3.76 (s, $\underline{H}_3$-CO) and δ_C 53.0 (O-$\underline{C}H_3$), which suggested the presence of a methoxyl group. The H_3-CO/C-6′ HMBC correlation allowed us to identify **4** as the methyl ester of pandaroside K. Compounds **5** and **6** were assigned as the methyl esters of **2** and **3**, respectively; in a manner similar to that used to assign the structure of compound **4**. These compounds may be formed from **1**–**3** during the extraction with MeOH. All relative and absolute configurations of compounds **2**–**6** were assumed to be the same as for previous pandarosides because of very similar NOESY and CD spectra.

3.2. Biological activity

3.2.1. Antiprotozoal and cytotoxic activity

Table 2 shows the *in vitro* antiprotozoal activity of the new compounds (**1**–**6**) against *T. b. rhodesiense*, *T. cruzi*, *L. donovani* and *P. falciparum*, as well as the cytotoxicity against rat skeletal myoblast (L6). Except for pandaroside M (**3**) and its methyl ester (**6**), which were inactive against *T. b. rhodesiense*, all these metabolites inhibited the growth of all four parasitic protozoa moderately and did not show cytotoxicity on mammalian cells. For comparison, antiprotozoal and cytotoxic effects of two previously isolated pandarosides, pandaroside G (**7**) and its methyl ester (**8**) are also included in Table 2.

On the other hand, compounds **1**–**6**, as well as previously isolated pandarosides [4,5] and acanthifoliosides [6], were tested for their antitumour activity (A549 lung cancer cells, HT29 colonic cancer cells, and MDA-MB-231 breast cancer cells). No activity was detected below 10 μM, with the exception of pandaroside G (**7**) and its methyl ester (**8**) (Fig. 1), which were active with GI_{50} values of 7.3 μM (A549), 6.7 μM (HT29) and 5.8 μM (MDA-MB-231) for compound **7**; and 0.3 μM (NSCL, HT29 and MDA-MB-231) for compound **8**. The same compounds were also toxic against L6 cells [5], hence these molecules may consequently be responsible for the initial antitumour activity of the crude extract and its subfractions.

Some structure–activity relationships (SARs) on the aglycone of pandaroside family had been drawn from previously results [5], however the exact impact of the position and the nature of additional sugar units remained unclear. In our results, the striking differences in the bioactivity of compound **2** and **7**, as well as **5** and **8**, which differ by the presence of a terminal xylose (Xyl) function at C-3′, clearly indicates that the xylose moiety is essential for their biological potential, increasing the antiparasitic and antitumour activities.

3.2.2. Haemolytic activity

A typical time drive of haemolysis is shown for acanthifolioside B (Fig. 3). Out of tested acanthifoliosides three, acanthifolioside A, B and D (**9**, **10** and **12**), showed strong haemolytic activity, with HC_{50} 15.0, 25.7 and 30.2 μM, respectively (Fig. 4). Acanthifolioside C showed only moderate haemolytic activity, while other metabolites of pandarosides and acanthifolioside families were not haemolytic. The time course of haemolysis and curve shapes point to the colloid-osmotic type of haemolysis for all three active acanthifoliosides. Initial lag phase of about 23–30 s is followed by very fast haemolysis with characteristic steep decrease of absorption. However, the structures of acanthifoliosides clearly resembles a typical saponin-like configuration and such compounds, mainly found in plants, holothurians and sea stars, are known to have surfactant-like activity on the biological membranes [13–15]. To estimate the approximate radius of putative pores we used a series of osmoprotectant molecules. While acanthifoliosides A and B expresses

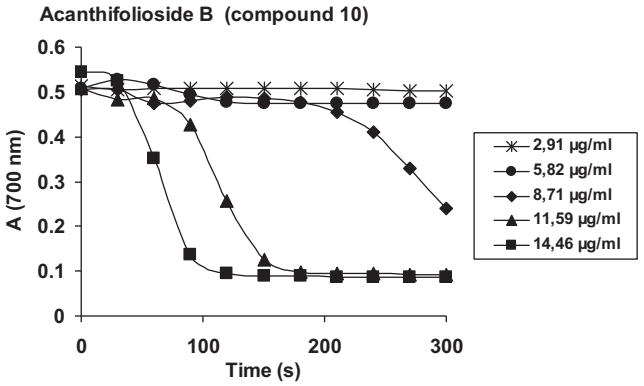

Fig. 3. A typical time course of haemolysis for tested acanthifoliosides. A lag phase of about 30 s is evident after addition of the compound. See Section 2 for further details.

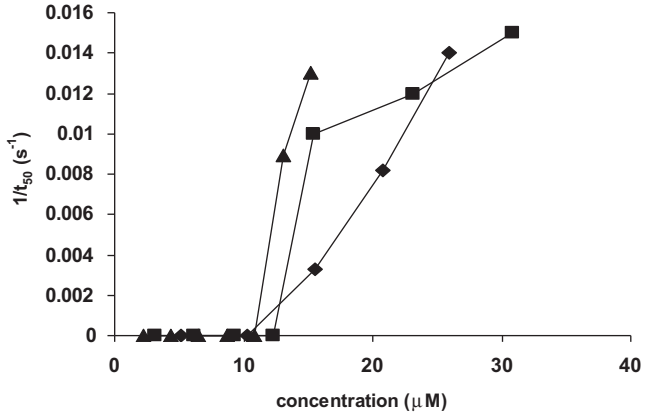

Fig. 4. The figure presents the velocity of haemolysis ($1/t_{50}$) for three different acanthifoliosides: B (compound 10, ♦), D (compound 12, ■) and A (compound 9, ▲). Note the exponential shape of curves obtained by acanthifolioside A and B which implies surfactant-like type of haemolysis, while that of acanthifolioside D is more sigmoidal characteristic for the colloid-osmotic type of lysis. Experimental details are described in Section 2.

Table 2
In vitro antiprotozoal and cytotoxic activities of sponge-derived compounds **1**–**8**. IC_{50} values are in μM.

Compound	*T. b. rhodesiense*[a]	*T. cruzi*[b]	*L. donovani*[c]	*P. falciparum*[d]	Cytotoxicity (L6 cells)[e]
Control drug	0.010[a]	2.64[b]	0.51[c]	0.2[d]	0.012[e]
1	71.9	68.0	63.1	28.7	>100
2	68.2	72.2	101.6	42.7	>100
3	>120	91.5	100.4	66.9	>100
4	63.4	61.4	63.1	28.4	>100
5	58.5	59.5	57.2	33.1	>100
6	>120	90.6	26.1	39.1	>100
7[f]	0.8	9.7	1.3	2.5	5.4
8[f]	0.038	0.77	0.051	0.39	0.22

[a] Melarsoprol.
[b] Benznidazole.
[c] Miltefosine.
[d] Chloroquine.
[e] Podophyllotoxin.
[f] Extracted from a previous work [5].

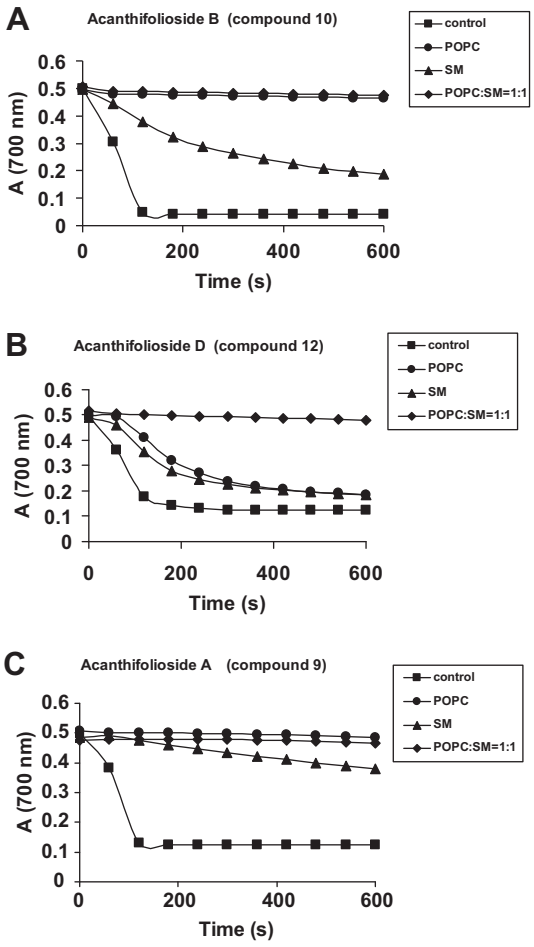

Fig. 5. Inhibition of haemolysis by small unilamellar lipid vesicles (SUV) composed of different lipids. Experimental details are described in Section 2.

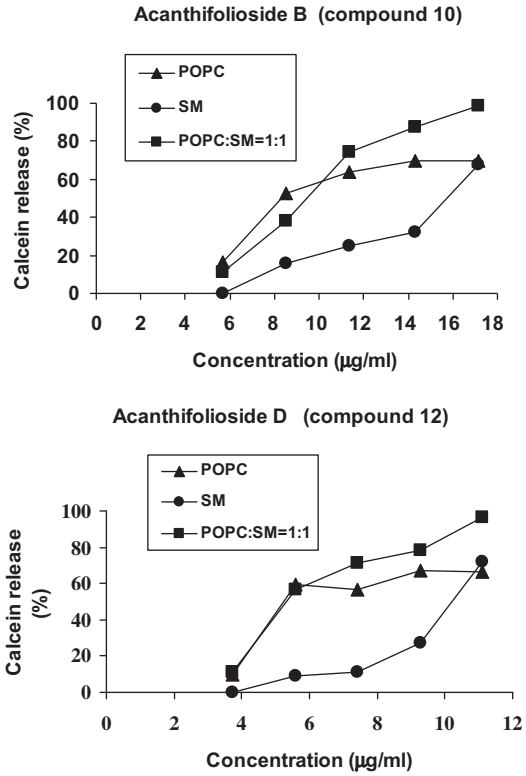

Fig. 6. Calcein release from SUV composed of different lipids and challenged with acanthifolioside B and acanthifolioside D, respectively. SUV were loaded with fluorescent dye calcein and its release was monitored upon addition of either compound. See Section 2 for further details.

similar pattern of osmoprotection and may cause haemolysis by formation of large but nevertheless defined membrane pores, acanthiofoliside D probably act similar to some detergent molecules since almost no protection was achieved even with largest osmoprotectant molecules (not shown). The estimation of pore diameter for other two compounds was not possible due to the fact that with osmoprotectants having larger hydrodynamic radius the haemolytic activities of acanthifoliosides A and B was almost completely blocked. After 10 min of measurements haemolysis did not reach half time of its value.

Observed differences in haemolytic activity could be explained by structural characteristics of tested compounds. As reported by Kalinin et al. [16] the membranotropic (haemolytic) activity of glycosides and their derivatives depends upon the position of the sulphate group in the carbohydrate chain, presence or absence of the 3-O-methyl group in terminal monosaccharide and peculiarities of aglycone structure.

Small unilamellar vesicles were used in order to reveal lipid specificity of haemolytic acanthifoliosides. A 1:1 POPC:SM mixture completely inhibited haemolytic activity of all three tested acanthifoliosides. POPC vesicles were equally effective in the case of acanthifolioside B and A, but much less in the case of acanthifolioside D. Acanthifoliosides B and D were only moderately inhibited by SM vesicles, while acanthifolioside A was strongly inhibited by SM vesicles, albeit slightly less as compared to the other two SUV preparations (Fig. 5).

Experiments with calcein loaded vesicles permeabilized with acanthifoliosides B and D showed that both compounds release calcein in similar extents at similar concentrations. However, acanthifolioside D was slightly more effective. Again, SUV composed of SM:POPC 1:1 mixture were most susceptible for permeabilization followed by those prepared of pure POPC. SUV prepared of pure SM were most resistant to permeabilization, but at the highest concentration of both tested acanthifoliosides they were permeabilized to the same extent as vesicles composed of POPC (Fig. 6). These results indicate that at least some of the acanthifoliosides might cause membrane disruption by a more specific and complicated mechanism than by simple surfactant-like activity.

Saponins are well known to exhibit cytotoxic and haemolytic activities [17], which are strongly correlated with the nature of both the aglycone and sugar side chains [18,19]. However, it was reported that these two properties are not linked since they can proceed by different mechanisms [20]. Pandarosides have showed the best antiprotozoal and cytotoxic profiles without haemolytic effect, while some acanthifoliosides (**9**, **10** and **12**) exhibited a strong haemolytic action. Interestingly, some acanthifolioside analogous found in starfishes, have been recognized as cytotoxins [21]. Thus, these findings indicate that the haemolysis could be one of chemical defenses of this sponge or its associate microorganisms against predators.

4. Conclusion

This study underlines and extends the large diversity of steroidal glycosides from marine sponges. The Caribbean *P. acanthifolium* produces two types of saponin glycosides, with differential antiprotozoal, haemolytic and cytotoxic potential. Some valuable SARs have been observed for this class of compounds. A medicinal chemistry approach might reduce the toxicity of some

pandarosides, such as pandaroside G (**7**) and its methyl ester (**8**), hence they might serve as lead compounds for further studies as antiprotozoal drug candidates. We did not find any membrane disrupting or haemolytic activities in pandarosides, but some of the acanthifoliosides show considerable haemolytic activity which might hinder the use of such compounds in clinical applications.

Acknowledgements

We are grateful to UNESCO and Boehringer Ingelheim Fonds for financial support provided by two fellowships (E.L.R.). We also thank Dr. J. Vacelet (Centre d'Océanologie de Marseille) for careful taxonomical sponge identification, M. Gaysinski and the PFTC of Nice for assistance in recording the NMR spectroscopic experiments, and Mr. le préfet de la Martinique and the DIREN for their help in the collection of Caribbean marine invertebrates.

Appendix A. Supplementary data

Supplementary data associated with this article can be found, in the online version, at doi:10.1016/j.steroids.2011.07.010.

References

[1] Munro MHG, Blunt JW. Marine Literatura DataBase (MarinLit). New Zealand: University of Canterbury; 2009.
[2] Berlinck RGS, Burtoloso ACB, Kossuga MH. The chemistry and biology of organic guanidine derivatives. Nat Prod Rep 2008;25:919–54.
[3] Schmitz FJ, Prasad RS, Gopichand Y, Hossain MB, Van der Helm D, Schmidt. Acanthifolicin, a new episulfide-containing polyether carboxylic acid from extracts of the marine sponge *Pandaros acanthifolium*. J Am Chem Soc 1981;103:2467–9.
[4] Cachet N, Regalado EL, Genta-Jouve G, Mehiri M, Amade P, Thomas OP. Steroidal glycosides from the marine sponge *Pandaros acanthifolium*. Steroids 2009;74:746–50.
[5] Regalado EL, Tasdemir D, Kaiser M, Cachet N, Amade P, Thomas OP. Antiprotozoal steroidal saponins from the marine sponge *Pandaros acanthifolium*. J Nat Prod 2010;73:1404–10.
[6] Regalado EL, Jiménez CM, Genta-Jouve G, Kaiser M, Tasdemir D, Amade P, et al. Acanthifoliosides, minor steroidal saponins from the Caribbean sponge *Pandaros acanthifolium*. Tetrahedron 2011;67:1011–8.
[7] Sepčić K, Kauferstein S, Mebs D, Turk T. Biological activities of aqueous and organic extracts from tropical marine sponges. Mar Drugs 2010;8:1550–66.
[8] Skehan P, Storeng R, Scudiero D, Monks A, McMahon J, Vistica D, et al. Comparison of in vitro anticancer-drug-screening data generated with a tetrazolium assay versus a protein assay against a diverse panel of human tumor cell lines. J Natl Cancer Inst 1990;82:1107–12.
[9] Macek P, Lebez D. Isolation and characterization of three lethal and hemolytic toxins from the sea anemone *Actinia equina* L. Toxicon 1988;26:441–51.
[10] Plaza A, Perrone A, Balesrieri ML, Felice F, Balestrieri C, Hamed AI, et al. New unusual pregnane glycosides with antiproliferative activity from *Solenostemma argel*. Steroids 2005;70:594–603.
[11] König WA, Benecke I, Bretting H. Gas chromatography separation of carbohydrate enantiomers on a new chiral stationary phase. Angew Chem Int Ed Engl 1981;20:693.
[12] Agrawal PK. NMR spectroscopy in the structural elucidation of oligosaccharides and glycosides. Phytochemistry 1992;31:3307–30.
[13] Thelestam M, Möllby R. Classification of microbial, plant and animal cytolysins based on their membrane-damaging effects of human fibroblasts. Biochim Biophys Acta 1979;557:156–69.
[14] Wang Y, Zhang Y, Zhu Z, Zhu S, Li Y, Li M, et al. Exploration of the correlation between the structure, hemolytic activity, and cytotoxicity of steroid saponins. Bioorg Med Chem 2007;15:2528–32.
[15] Van Dyck S, Gerbaux P, Flammang P. Qualitative and quantitative saponin contents in five sea cucumbers from the Indian ocean. Mar Drugs 2010;8:173–89.
[16] Kalinin VI, Prokofieva NG, Likhatskaya GN, Schentsova EB, Agafonova IG, Avilov SA, et al. Hemolytic activities of triterpene glycosides from the holothurian order Dendrochirotida: some trends in the evolution of this group of toxins. Toxicon 1996;34:475–83.
[17] Sparg SG, Light ME, van Staden JJ. Biological activities and distribution of plant saponins. J Ethnopharmacol 2004;94:219–43.
[18] Oda K, Matsuda H, Murakami T, Katayama S, Ohgitani T, Yoshikawa M. Adjuvant and haemolytic activities of 47 saponins derived from medicinal and food plants. Biol Chem 2000;381:67–74.
[19] Takechi M, Tanaka Y. Haemolytic time course differences between steroid and triterpenoid saponins. Planta Med 1995;61:76–7.
[20] Gauthier C, Legault J, Girard-Lalancette K, Mshvildadze V, Pichette A. Haemolytic activity, cytotoxicity and membrane cell permeabilization of semi-synthetic and natural lupane- and oleanane-type saponins. Bioorg Med Chem 2009;17:2002–8.
[21] Izzo I, de Riccardis F, Sodano GJ. Synthesis of (25R)-5alpha-cholestane-3beta, 6beta, 15alpha, 16beta, 26-pentol, a cytostatic starfish steroid. J Org Chem 1998;63:4438–43.